EES Solar

PAPER

View Article Online
View Journal | View Issue

Cite this: *EES Sol.*, 2025, **1**, 543

Pow(d)ering up: FAPI perovskite nanopowders for air-processed blade coated perovskite solar modules†

Maurizio Stefanelli,[a] Muhammed P. U. Haris,[b] Luigi Vesce,[acd] Luigi A. Castriotta,[a] Hafez Nikbakht,[a] Fabio Matteocci,[a] Samrana Kazim,[bef] Alessandro Triolo,[g] Shahzada Ahmad *[bf] and Aldo Di Carlo *[ag]

Formamidinium lead iodide (FAPI) is the most prominent perovskite material utilized in the fabrication of single-junction perovskite solar cells. However, the cubic α-phase perovskite is difficult to retain in precursor solutions for extended periods due to thermodynamic instability, which promotes the formation of the yellow δ-phase. In this study, we demonstrate the fabrication of solar cells and modules from FAPI powders synthesised using a single-step method with a non-hazardous solvent and routine purity grade lead iodide. The pre-synthesised α-FAPI and CsFAPI powders demonstrated considerable potential for scalability and reproducibility. It was observed that similar efficiencies were achieved in small-area cells and mini-modules fabricated using an industrially adaptable blade coating process conducted in an open environment. The enhanced solution rheology and the meticulous control of stoichiometry result in an oriented and less strained crystal lattice, thereby demonstrating superior reproducibility and stability of the perovskite prepared from pre-synthesised powder in comparison to the one produced from high-purity precursor. The methodology developed offers a scalable and cost-effective approach to the production of high-performance and stable perovskite solar modules, with efficiencies reaching 18.5% on a 12.15 cm^2 active area module and a T95 above 1200 h in shelf life stability at 30% RH in a UV-filtered environment.

Received 13th March 2025
Accepted 28th June 2025

DOI: 10.1039/d5el00032g

rsc.li/EESSolar

Broader context

Halide Perovskite (PVSK) Photovoltaics (PV) are moving from laboratory to pilot/production lines. The success of this transition is based on the use of stable formulation of PVSK and scalable coating techniques preferably in ambient air. Despite big efforts in the scaling up of PVSK technology in the literature, few works faced module fabrication entirely in ambient air. Furthermore, high purity raw materials for PVSK precursor solution and manual handling of them are critical points for the fabrication costs and the reproducibility of the stock solutions. In this work, we show the scaling up of PSC technology by a double step meniscus coating process out of a glovebox with green antisolvent quenching. The entire stack till HTL (nip configuration) is made in ambient air and with scalable techniques. In addition, we make use of pre-synthesised cesium-containg FAPI powder obtained by a single step synthesis with green solvent at room temperature and with low-cost and purity lead iodide. According to our knowledge, this work presents the first FAPI powder made from low-cost lead iodide employed in a fully ambient air fabrication method.

Introduction

The growth of single junction perovskite-based photovoltaics is being driven by formamidinium lead iodide (FAPI) based perovskites. The high carrier mobility and optimal bandgap, as predicted by the Schottky–Queisser limit, are reflected in exceptional efficiencies above 26% for both p-i-n and n-i-p type solar cell configurations.[1–3] In comparison to other halide perovskites, the absence of bromine ions and the use of methylammonium (MA^+) cation only for cubic α-phase stabilisation (*e.g.* MACl) contribute to the enhanced stability of the film. The stability of the film is considerably improved due to the absence of phase segregation and the higher temperature stability of the formamidiunium cation (FA^+) for MA^+.[4,5] The general route for

[a]*CHOSE, Department of Electronic Engineering, University of Rome "Tor Vergata", 00133 Rome, Italy. E-mail: aldo.dicarlo@uniroma2.it*

[b]*BCMaterials - Basque Center for Materials, Applications and Nanostructures, Martina Casiano, UPV/EHU Science Park, Leioa, 48940, Spain. E-mail: shahzada.ahmad@bcmaterials.net*

[c]*Department of Biomedicine and Prevention, University of Rome "Tor Vergata", 00133 Rome, Italy*

[d]*Department of Physics, University of Rome "Tor Vergata", 00133 Rome, Italy*

[e]*Materials Physics Center, CSIC-UPV/EHU, Paseo Manuel de Lardizabal 5, 20018 Donostia-San Sebastian, Spain*

[f]*IKERBASQUE, Basque Foundation for Science, Bilbao, 48009, Spain*

[g]*ISM-CNR, Consiglio Nazionale delle Ricerche, 00133 Rome, Italy*

† Electronic supplementary information (ESI) available. See DOI: https://doi.org/10.1039/d5el00032g

FAPI or FA-rich perovskite deposition requires high-purity precursors (*e.g.* PbI_2/FAI) dissolved in different solvents depending on whether the anti-solvent or the double step method is used.[6–10] The anti-solvent or double step method is a conventional approach to preparing perovskite solutions. However, errors in the precise weighing of precursor materials may result in the formation of non-stoichiometric species (cations, halides) in the solution, leading to non-radiative losses and reduced efficiencies.[11,12] Additionally, the rheological properties of the solution are a critical consideration. The colloids in perovskite precursors consist of a series of iodoplumbate complexes $[PbIn]_{(n-2)}$ as building blocks for large-size self-assembled lead polyiodides frameworks, which are linked by Pb–I–Pb corner-sharing coordination.[13] It has been observed that, in the standard solution-making route, colloids are much smaller than perovskite solutions prepared from pre-synthetized powders. The larger lead polyiodides frameworks in the latter case led to a preferable and oriented crystallisation of the perovskite layer.[14]

For these reasons, pre-synthesized pure α-FAPI or CsFAPI powders have demonstrated high potential in ensuring device stability and reproducibility as well as efficiency.[15,16] The synthesis can be carried out in different solvent media, including 2-methoxyethanol, acetonitrile, or even in an aqueous solution with high yield (>90%).[1,17–20] After the precipitation step, the powder is filtered, annealed at 150 °C, washed with orthogonal solvents (*i.e.* diethyl ether, chlorobenzene) and kept in a vacuum atmosphere to extract the solvent traces. The synthesised powder can be processed in a typical solvent mixture (DMF/DMSO, 2-ME/NMP) and employed as a perovskite precursor ink. It has been demonstrated that perovskite crystals/powders are superior for exact-stoichiometry perovskite films with lower defects, resulting in highly uniform and efficient perovskite solar cells exceeding 24% PCE.[21] Furthermore, the precursor solution obtained from the powder exhibits a longer shelf-life than the standard one.[15]

The precise control of the stoichiometry of the powder methodology is reflected in higher reproducibility and performance compared to the raw precursor's counterpart, thereby demonstrating the benefits of obtaining FAPI powders from low-purity precursors (PbI_2) without performance loss.[22,23] This approach to FAPI synthesis, involving batch production from low-purity precursors without the need to weigh each one individually from batch to batch, is well suited to an industrial context thanks to its favourable balance of cost and efficiency. Furthermore, compositional engineering is paramount to push stability, and cesium incorporation can allow the formation of Cs-FAPI, which possesses higher stability according to the Goldschmidt tolerance factor.[24] Enhanced operational and moisture stability are demonstrated as well as milder temperature to α-phase transition with respect to the cesium-free counterpart.[18,19,21,24–27]

In this context, pre-synthetized α-FAPI powder is emerging as a material for large area devices. Jiang *et al.* employed low-purity PbI_2 precursor material to synthesize $FAPbI_3$ in 2-methoxy ethanol solvent (2-ME) *via* inverse temperature crystallization and fabricated corresponding solar cells and mini-modules through spin-coating inside the glove box. The best-performing device measured an efficiency of 23.9% on small area devices and 19.5% on 13.44 cm^2 mini-module active area.[28] Moreover, the cells retained more than 95% of the initial power conversion efficiency (PCE) after 400 h of storage in shelf-life conditions. Further, Tong *et al.* proposed a method to avoid impurities from powder synthesis using hydroiodide acid, formamidiunium acetate, lead iodide, and γ-butyrolactone, and defect-less FAPI perovskite films were fabricated through solubility management. The best-performing spin-coated device displayed an efficiency of 23% and 16% for a small area and 22 cm^2 active area module, respectively.[17] Recently, Du *et al.* have emploied CsFAPI single crystals as perovskite precursors underlying the impact of colloids and volatile solvents for effective and homogeneous nucleation. The suppressed secondary nucleation and extended growth of crystals enable high throughput fabrication of full printed carbon-based devices in a controlled environment (RH < 5%) with an efficiency of 19.3% and 16.2% on a small area and 16.84 cm^2 active area mini-module, respectively.[29]

FAPI powders are a promising material for module fabrication, but have only been used thus far in a controlled atmosphere within a glove box. There are currently no reports on the scaling up of this process to module size in ambient air. The objective of this work is to address this gap by demonstrating the fabrication of modules in ambient air using pre-synthesized powders. In order to achieve this objective, we have selected $Cs_xFA_{1-x}PbI_3$ perovskite powder (CsFAPI-pw), with a cesium content (x) of less than 10%, which has been synthesised with one-pot synthesis in a non-hazardous solvent with a yield >93%. We compared powders obtained with low-purity lead iodide sources and those from conventional high-purity precursors (CsFAPI-hp) used for small-area cells and mini-module fabrication. Here, all the layers (except for gold) in both small area (0.5 cm^2 active area) and minimodules (12.5 cm^2 active area) devices were deposited in ambient air by blade coating technique, with a commendable efficiency for small area (0.5 cm^2) cells of 19.4% and 19.2% obtained from $Cs_xFA_{1-x}PbI_3$ pre-synthetized powder and conventional precursor route, respectively. The perovskite films obtained with the powder method exhibit superior performances in terms of efficiency, stability (ISOS-D1), and reproducibility. We then selected CsFAPI-pw for mini-module fabrication and the device measured 18.5% (less than 5% losses with respect to the small area cell) on a 12.5 cm^2 active area.

Results and discussion

The deposition of the perovskite layer by solution process is achieved by dissolving the precursors (*e.g.* FAI and PbI_2) in a mixture of solvents (*e.g.* DMF/DMSO) and subsequently depositing them as a thin film. Although there are reports of using the perovskite powder in the fabrication of perovskite solar cells (PSCs), the use of meniscus coating, such as blade coating, has not been explored in the context of fully ambient air device fabrication.[30,31] In this study, black CsFAPI powder (Fig. 1a and b) was used as a precursor material for perovskite with blade coating technique (Fig. 1c).[27] A conventional perovskite ink was also prepared from high-purity PbI_2, CsI, and FAI for comparative purposes.[32] The rheology of the two solutions

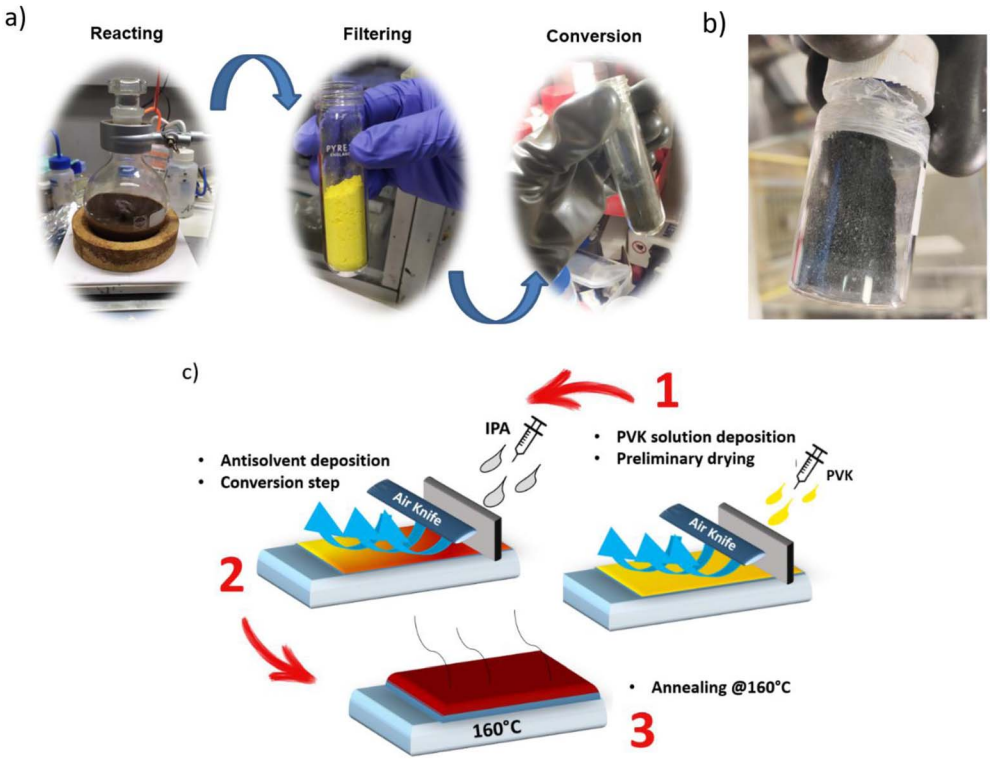

Fig. 1 CsFAPI powder synthesis steps (a); black CsFAPI powder (b); process routine for CsFAPI perovskite deposition in ambient air with blade coating technique (c).

was characterised using dynamic light scattering (DLS) measurement. DLS experiment have been performed to assess the average diameter size of the aggregates present in both CsFAPI-hp and CsFAPI-pw solutions. The population of the colloids in the precursor and powder solutions demonstrates that the size of the particles is influenced by the starting precursor material. In the case of CsFAPI-hp solution, only small-size colloids (~1 nm) were detected (Fig. 2a). In contrast, CsFAPI-pw solution exhibited a notable population of colloids in the order of 100 nm, constituting 20% of the total DLS intensity (Fig. 2b). The larger size of the colloids wich are attributed to the iodoplumbate complexes $[PbI_n]_{(n-2)}$ may have an impact on the film crystallization process, acting as seeds during the fabrication step.[33–35] Besides the small colloids acting as nucleation sites and subsequently undergo a diffusion-controlled growth as described by the LaMer mechanism,[36] the larger colloids in the CsFAPI-pw case can drive oriented growth.[14] The discrepancy between the two population sizes can effectively alter the solution chemistry resulting in the formation of a higher-quality and less strained crystalline film,

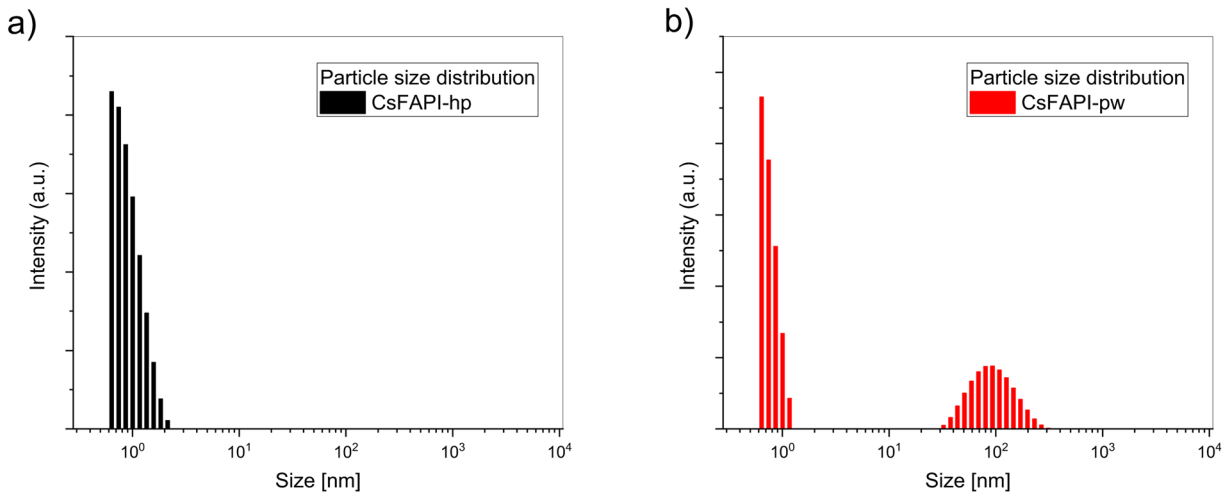

Fig. 2 Particle size distribution for CsFAPI-hp (a) and CSFAPI-pw solution, and (b) measure by dynamic light scattering technique.

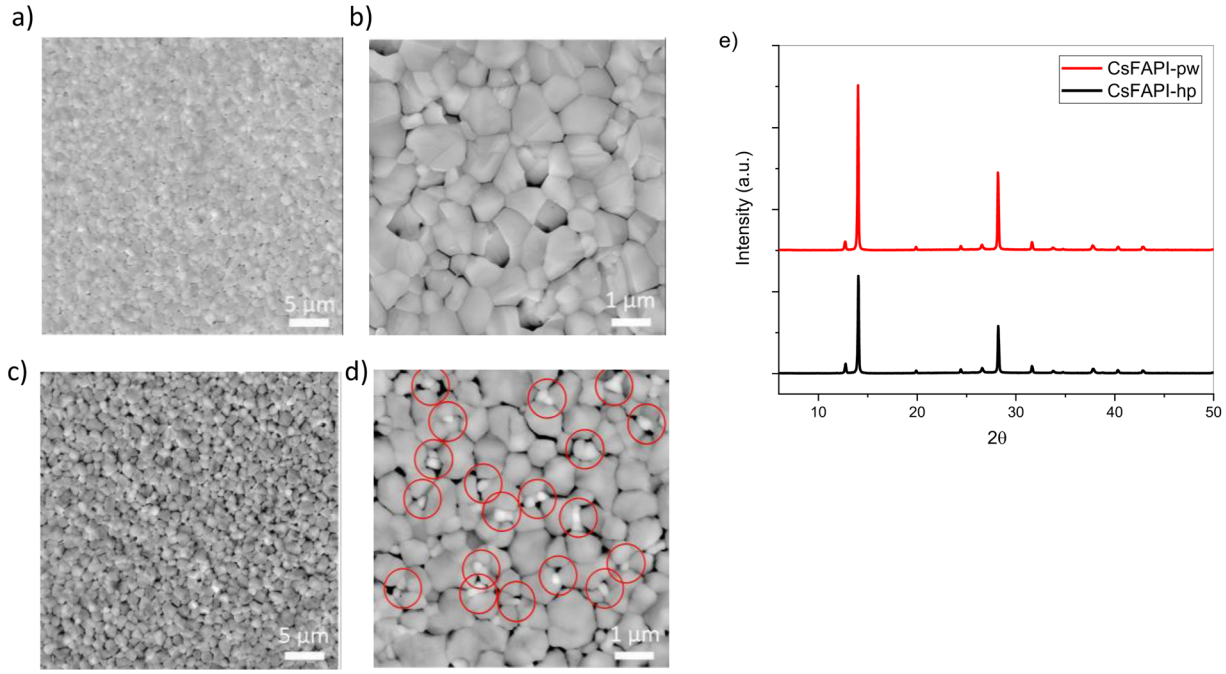

Fig. 3 SEM top view of CsFAPI-pw (a and b) and CsFAPI-hp (c and d) at lower and higher magnification, respectively; red circles in Fig. 2d highlight unreacted PbI_2; XRD diffraction pattern of CsFAPI-hp and CsFAPI-pw deposited by blade coating on bare FTO (e).

as confirmed also by XRD peak analysis. CsFAPI films in both cases were fabricated *via* the blade coating technique in an ambient atmosphere with isopropanol green-solvent quenching followed by annealing at 160 °C for 10 min (Fig. 1b) as previously described.[37] The thin films fabricated from perovskite powder and conventional precursors are labelled hereafter as CsFAPI-pw and CsFAPI-hp, respectively.

To compare the quality of CsFAPI-pw to the CsFAPI-hp, we fabricated and characterized a small area (0.5 cm^2 a.a.) PSCs and films coated on a 5 × 5 cm^2 substrate, and were cut into four smaller pieces (2.5 × 2.5 cm^2) prior to the thermal evaporation of the back electrode. The morphological analysis (Fig. 3) indicates that the CsFAPI-pw exhibits superior uniformity compared to the CsFAPI-hp. Micron-size grains are detected for CsFAPI-pw presenting a compact and pinholes-free (Fig. 3a and b) film due to the different crystallization profiles of nucleation rate and crystal growth. On the other hand, CsFAPI-hp shows smaller grains and the presence of unreacted PbI_2 (Fig. 3c and d) that can compromise the film quality and stability over time. The X-ray diffraction (XRD) patterns for both CsFAPI films (Fig. 3e) show peaks at $2\theta = 14°$ and 28°, which are indicative of perovskite orientation along (00*h*) facets that have been identified as the desired orientation for solar cell applications.[38] It should be notice that lead iodide signal at 12.6° is still present for CsFAPI-pw even if there are not possible excess in the stoichiometry of the solution. The reason of that behave in the antisolvent quenching. Infact IPA it's a well know green antisolvent and recently integrated also as passivator additive in other antisolvent system (*i.e.* chlorobenzene) and eventually used as a washing step to provoke the 2D crystals reorganization on the surface of 3D perovskite.[39–41] In this work bare IPA is used as antisolvent and of curse a large excess of IPA in the antisolvent system can produce some lead iodide[39–42] that is treated and washed out with the passivation strategy with PEAI to form 2D perovskite and wash out the unreacted lead iodide as we already described in a previous work on passivation strategy.[43]

While the intensity of diffraction peaks is higher for the CsFAPI-pw as compared to CsFAPI-hp suggesting an enhanced crystallinity as well as a larger lattice constant as indicated by the shift toward lower 2θ in the diffractograms (Fig. 3e). In a previous work, we attributed the enhanced crystallinity of the powder-processed $FAPbI_3$ films deposited by the spin coating technique, to their conventional counterpart to reduced microstrain.[18] To assess the impact of the microstrain on the blade-coated thin films and to evaluate how it translates to large-scale fabrications, we performed a detailed analysis of the diffraction peaks employing the Williamson–Hall[21] equation

$$\beta \cos\theta = \frac{k\lambda}{D} + 4\varepsilon \sin\theta \quad (1)$$

where β, λ, k, D, and ε denote the full width at half-maximum of the diffraction peak, the wavelength of X-ray radiation, the Scherrer constant, the crystallite size, and the microstrain, respectively. We plotted $\beta \cos\theta$ as a function of 4 $\sin\theta$, and the slope calculated from the linear fitting was estimated as the microstrains (Fig. S1†). We found that, besides the enhanced crystallinity, the CsFAPI-pw film displays a lower microstrain value of 6×10^{-4}, while the conventional CsFAPI-hp counterpart shows a higher value of 6.54×10^{-4} (Fig. S1†). The reduced microstrain will induce long-term stability and the efficiency of CsFAPI-pw devices due to the impact of microstrain on structural stability, defect generation, charge carrier dynamics, and local disorder near the band edges.[18,21,44,45]

Photovoltaic performances & dynamic light scattering

We evaluated the photovoltaic performances of the small area devices using a planar n-i-p architecture, composed of FTO/SnO_2/PVK/PEAI-passivation/Spiro-OMeTAD/Gold. Fig. 4a–d show the statistics on photovoltaic parameters for 15 devices (CsFAPI-pw and CsFAPI-hp). The mean value and the standard deviation of V_{oc}, J_{sc}, FF, and PCE show a dramatic improvement in the reproducibility and efficiency of CsFAPI-pw with respect to CSFAPI-hp devices (Table 1). Moreover, the absence of unreacted species and the less strained crystal lattice improve

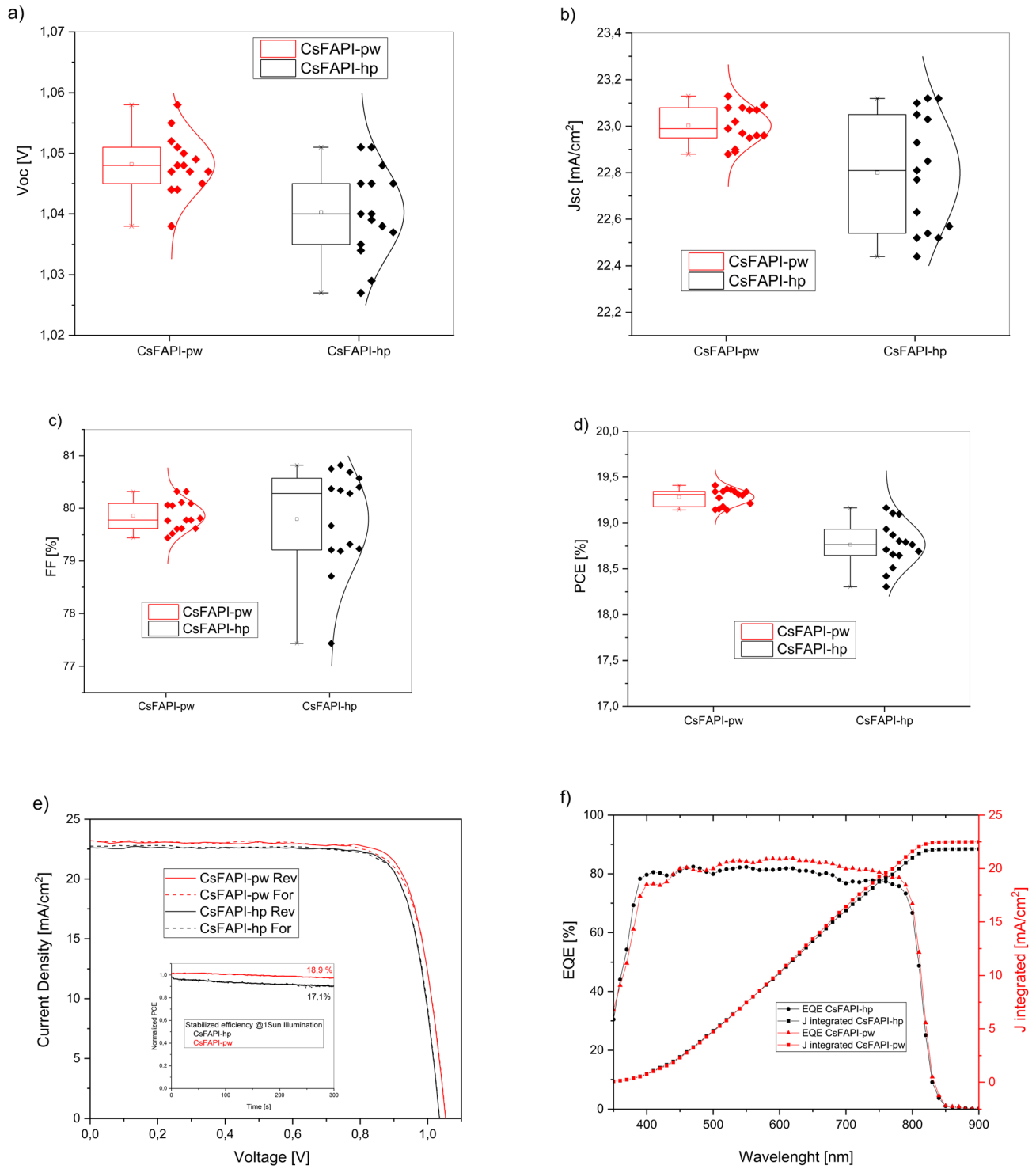

Fig. 4 Statistics of photovoltaic parameters for CsFAPI-hp and CsFAPI-pw devices: V_{oc} (a) J_{sc} (b) FF (c) and PCE (d); J–V curves for the record devices of CsFAPI-hp and CsFAPI-pw respectively on 0.5 cm^2 active area (e); EQE of the best devices (f).

Table 1 Mean values and standard deviation over 15 devices fabricated with CsFAPI-pw and CsFAPI-hp of photovoltaic properties for the fabricated devices

	V_{oc} [V]	J_{sc} [mA cm^{-2}]	Fill factor [%]	PCE [%]
CsFAPI-pw	1.048 ± 0.004	23.000 ± 0.080	79.860 ± 0.079	19.141 ± 0.008
CsFAPI-hp	1.040 ± 0.007	22.800 ± 0.248	79.790 ± 0.902	18.304 ± 0.061

stability over time and robustness during the ambient air fabrication process.[22] The champion devices with 0.5 cm^2 active area for CsFAPI-pw showed open circuit voltage (V_{oc}) of 1.05 V, short-circuit current density (J_{sc}) of 23.07 mA cm^{-2}, fill factor (FF) of 79.89%, and PCE of 19.40%. While, CsFAPI-hp displayed V_{oc} of 1.05 V, J_{sc} of 22.66 mA cm^{-2}, FF of 80.4%, and PCE of 19.03%. In both cases, the devices showed negligible hysteresis (Fig. 4e). Short circuit current is in agreement with integrated J_{sc} in EQE measurement where CsFAPI-pw has a higher conversion in the wavelength range 500–820 nm (Fig. 4f).

To investigate the improvement of average V_{oc} in CsFAPI-pw concerning CsFAPI-hp and its relation with perovskite properties such as trap densities, we carried out space charge limit current (SCLC) and transient photoluminescence (TRPL) analyses to evaluate and compare the trap state densities of both perovskite films. SCLC measurements were carried out with an electron-only device architecture, namely FTO/SnO_2/PVK/PCBM/Ag.[46] The trap-filled limit (TFL) voltage (V_{TFL}), (Fig. 5a), was determined from the change of slope between the ohmic region ($n \approx 1$) and the TFL region ($n > 2$). CsFAPI-pw showed significantly reduced V_{TFL} (0.233 V) for that of CsFAPI-hp (0.442 V). This proves the better quality of the film also in the bulk and it's reflected in the higher overall photovoltaic

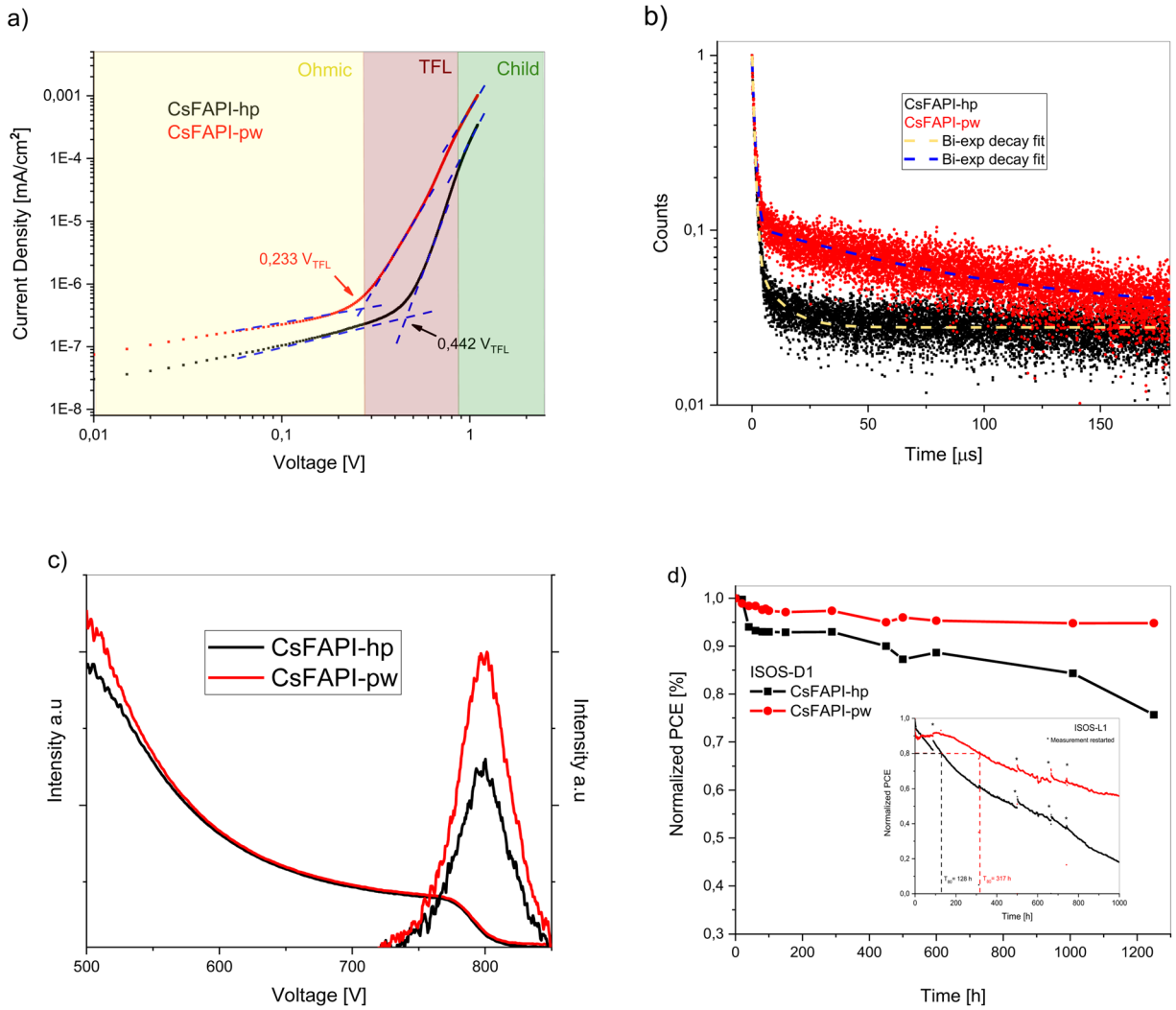

Fig. 5 SCLC analysis (a), transient photoluminescence decay (b), UV-Visible spectra and PL measurements of PVK films (c) and ISOS-D1 at 30% RH in UV-filtered box for CsFAPI-hp and CsFAPI-pw (d), respectively.

Table 2 TRPL double exponential fit for decay of CsFAPI-pw and CsFAPI-hp perovskite films

Sample	A_1	τ_1 [μs]	A_2	τ_2 [μs]	τ_{ave} [μs]	A_0
CsFAPI-hp	0.955	0.947	0.039	9.706	1.29	0.027
CsFAPI-pw	0.845	1.043	0.070	75.168	6.77	0.033

performances of the CsFAPI-pw devices. The trap state density (N_{trap}) can be estimated with the following equation:[47]

$$N_{traps} = \frac{2V_{TFL}\varepsilon_0\varepsilon}{eL^2} \quad (2)$$

where N_{traps}, V_{TFL}, ε_0, ε, e, L are trap-state density, the trap-filed limit voltage, vacuum permittivity ($\varepsilon_0 = 8.8 \times 10^{-12}$ F m^{-1}), the relative dielectric constant of perovskite (with reference to 62.23), electron charge ($e = 1.6 \times 10^{-19}$ C), the film thickness of perovskite (800 nm), respectively. Since perovskites with the same stoichiometry and thickness have the same ε_0, ε, e, and L, the magnitude of N_{trap} is only determined by V_{TFL}. N_{trap} determinations were 4.75×10^{15} cm^{-3} for CsFAPI-hp and 2.5×10^{15} cm^{-3} for CsFAPI-pw, thus further endorsing the potential of pre-synthetized powder to obtain thin-film with less trap state density and low hysteresis in PSCs.[48] Further, TRPL characterization was performed on both perovskite films (sample stack Glass/FTO/PVK) with 405 nm pulsed diode laser, and a double exponential fit was applied to determine their average decay times, as reported in Table 2.

$$\frac{\Delta T}{T}(t) = A_1 e^{-\left(\frac{t}{\tau_1}\right)} + A_2 e^{-\left(\frac{t}{\tau_2}\right)} + A_0 \quad (3)$$

$$\tau_{ave} = \frac{A_1\tau_1^2 + A_2\tau_2^2}{A_1\tau_1 + A_2\tau_2} \quad (4)$$

Assuming that τ_{ave} is affected by the trap density and the corresponding lifetime of the free carriers generated into the film,[49] is in agreement with SCLC analysis and with the higher peak of photoluminescence (performed on Glass/FTO/PVK sample, excitation wavelength 385 nm) on CsFAPI-pw with respect to the CsFAPI-hp (Fig. 5a–c).

Furthermore, we assess the shelf-life stability of both non-encapsulated perovskite devices performing ISOS-D1 at 30% RH in a UV-filtered environment.[50] CsFAPI-hp-based perovskite shows a significant efficiency drop (Fig. 5d) in the first 100 hours and presents a large degradation trend starting from 600 hours with a reduction of 20% of initial efficiency (T_{80}) of 1100 h. On the other hand, CsFAPI-pw based perovskite, which is characterized by a smooth and compact film with low defects and low content of unreacted species on its surface, can resist under 30% RH for more than 1200 hours, losing only less than 5% of its initial efficiency.

To further test the stability of the perovskite layer we conducted ISOS-L1 stability test in ambient air at 35/40 °C on encapsulated devices with UV-curable resin. The stack is (FTO/SnO_2/PVK/PEAI/Spiro-OMeTAD/Au). As shown in the inset of Fig. 5d, the first drop in efficiency is visible for both perovskite formulations due to the burn-in effect and encapsulation process, which slightly decrease efficiency within the first 24 hours of light exposure.[51,52] The CsFAPI-hp device reach the T_{80} only after 128 h of light exposure, as result of the poor crystallinity of the PVK film and the elevated lead iodide excess that affect the operational stability.[53,54] In the CsFAPI-pw case, the stability is more than doubled (T_{80} = 317 h) respect to the CsFAPI-hp devices, highlighting the improved operational stability of the layer. Moreover, after 1000 h of test the CsFAPI-pw device lose a bit less than 40% of the initial efficiency where instead the CsFAPI-hp device efficiency dropped more than 80% respect the initial efficiency. PVK layer obtained from nano powder still suffers from the pinholes (smaller and in lower quantity, but stil present) into the PVK film as shown in the SEM top view images (Fig. 3a and b). The possible reasons of that can be found in the massive quantity of IPA used onto the super-saturated PVK film in the deposition process that extracts part of the formamidiunium that is highly soluble in alcoholic solvents.[39,40,42] Should be pointed out that no additives are used in the PVK layer except for MACl that helps to stabilize the alpha phase in the deposition process.[55] The stability obtained is in line with our previous work on PVK film obtained from powders with similar architecture[18] but further improvements with antisolvent engineering and additives selection are needed to reach the optimal operational stability.

Based on the remarkable results obtained on small-area cells, we scale up the fabrication process used in small-area cells to realize mini-modules. Considering the improved reproducibility and stability for CsFAPI-hp, we focused only on the CsFAPI-pw perovskite for such a study. The mini-module has a total active area of 12.5 cm^2 and a geometrical fill factor (GFF) of 93%, giving an aperture area of 13.44 cm^2. P1–P2–P3 laser scribing scheme[56] was adopted during the fabrication process to guarantee the series Z connection among the 5 sub-cells (2.5 cm^2 active area each) of the mini-module. The SEM/EDX and the scheme of the P1–P2–P3 laser process are presented (Fig. 6a and b). The relative small signal of lead, carbon, iodine, and the strong signal from tin and oxygen inside P2/P3 etching lines from the EDX mapping confirmed the good quality of the laser process in the removal of the stack without damaging TCO. The best-performing mini-module (Fig. 6c) displayed a V_{oc} of 1064 mV for each cell, 52 mA of current, 76% FF, and a PCE of 18,46% (17.17% on aperture area) in the reverse scan. For the forward scan, the PCE was slightly improved to 18.5% (17.2%). Negligible hysteresis and high reproducibility achieved in this process attest to the potential of our powder engineering strategy for module fabrication. The optimization of the P2 laser process contributed to the high-quality contact with the TCO (75% fill factor of), negligible hysteresis, and less than 5% efficiency difference with small area devices.[43,48,57,58]

We made preliminary cost estimations for the CsFAPI-pw and CsFAPI-hp, and the data referred to the material usage are normalized to 1 g of perovskite. In the case of CsFAPI-pw, the costs of the solvents are considered for the reaction (acetonitrile, ACN) and for washing the synthesized product

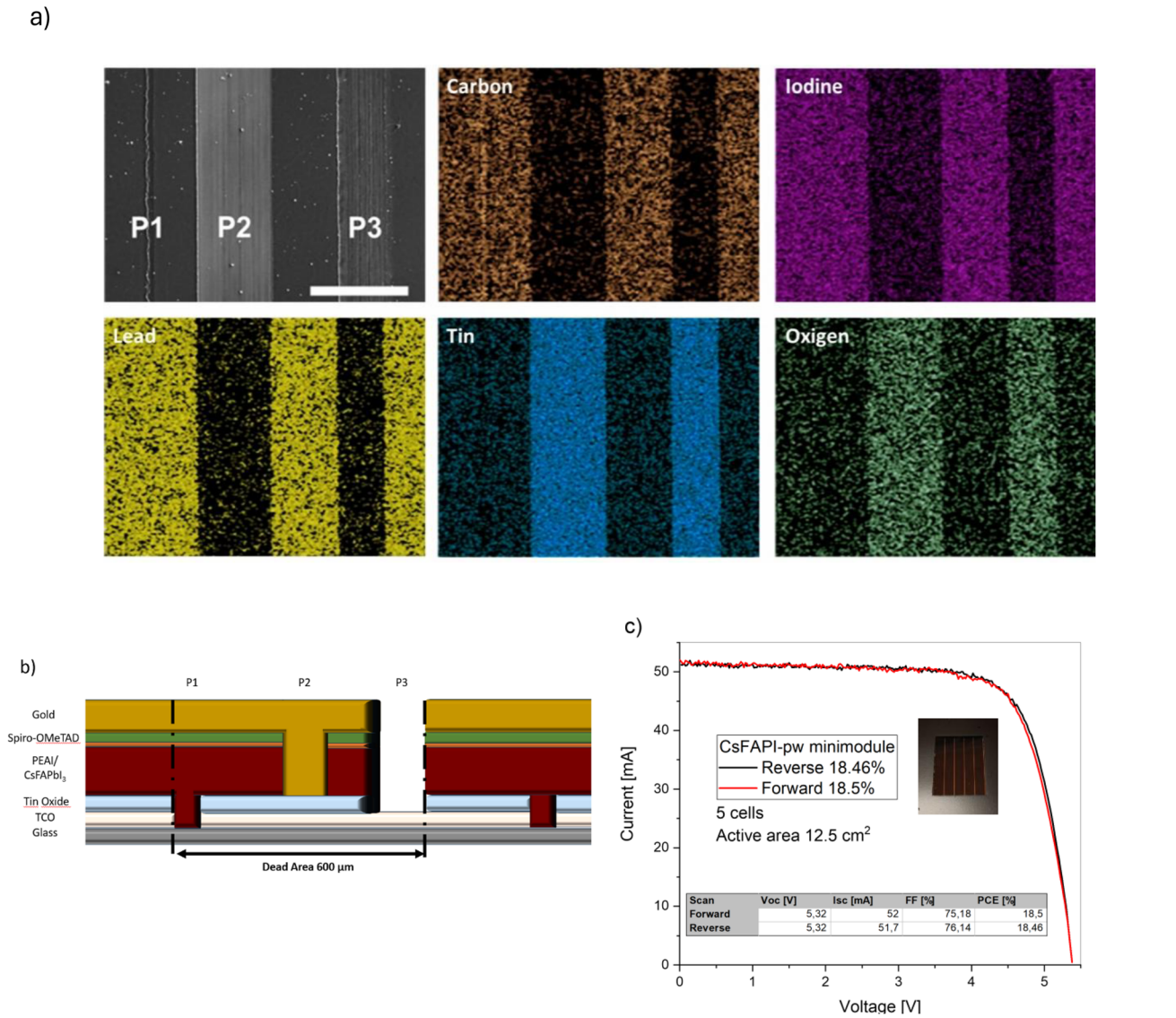

Fig. 6 Minimodule Image and EDX analysis of P1–P2–P3 scribing process (scale bar is 250 µm) (a); cross view of P1/P2/P3 process in stack and dead area (b) *I–V* curve of the best minimodule made with CsFAPI-pw precursor (c).

(diethyl ether) (Tables S1 and S2†). With a rough estimation of the costs and a yield set at 100% for CsFAPI-hp as estimated, considering the "direct synthesis" during the deposition, and 93% for CsFAPI-pw (empirically determined by weighing the converted black FAPI powder and extracting the moles of product useful for the yield calculation $\text{moles}_{\text{product}}/\text{moles}_{\text{reagents}} \times 100$), the overall costs for 1 g of perovskites is one fourth for CsFAPI-pw compared to the cost of CsFAPI-hp. This demonstrates the economic sustainability of the FAPI powder made from low-purity lead iodide, which can play a game-changer role in the manufacturing costs. Further, CsFAPI-pw can be produced in a batch production eliminating the need for multiple powder weighing and possible manual errors that can occur in the process and affect the stoichiometry of the solution and will promote reproducibility.

Conclusion

In conclusion, the utilisation of pre-synthetised Cs-$FAPbI_3$ powder in conjunction with a scalable deposition technique, blade coating, under ambient air conditions, has been demonstrated for the fabrication of both small-area cells and modules. The photophysical characterisation of the resulting films demonstrates the superior quality of the perovskite layers produced from the pre-synthetized powder source. The fabricated small-area cells and mini-modules exhibit low hysteresis and efficiency losses of less than 5% when scaling from 0.5 cm^2 to 12.5 cm^2 active areas, along with a shelf-life stability exceeding 1200 hours, retaining over 95% of their initial efficiency. The presented methodology demonstrates that the use of high-purity lead iodide is not a prerequisite for the

fabrication of stable and high-efficiency devices, thereby offering a significant reduction in production costs.

The next crucial phase for perovskite solar cell technology is the industrial production of solar modules. In this context, it is essential to prioritise the optimisation of fabrication costs, economic viability and environmental sustainability, alongside the enhancement of device performance. This work represents the inaugural demonstration of the utilisation of low-cost materials, batch production, green solvents (for synthesis and for the antisolvent step), and scalable techniques under ambient conditions, all of which are indispensable elements for the industrialisation of perovskite technology. The powder engineering approach, which employs ambient blade coating, offers a promising pathway to addressing these challenges. The reliability and sustainability of the processes are further reinforced through the use of green solvents for perovskite precursor synthesis (ACN) and antisolvent quenching (Isoprpanol, IPA), as well as the use of low-purity precursors (lead iodide) and ambient air fabrication methods.

Data availability

Data for this article, including EQE, UV-Vis, JV and DLS measurements are available at ZENODO repository at (**https://doi.org/10.5281/zenodo.14164839**).

Conflicts of interest

There are no conflicts to declare.

Acknowledgements

M. P. U. H. acknowledges the support of the H2020 Project "VIPERLAB" of European Union (no. 101006715). SA acknowledges support for the European Research Council Consolidator grant [MOLEMAT, 726360]. And also the Spanish Ministry of Science and Innovation INTERACTION {PID2021-129085OB-I00} and CNS2022-136171 funded by MCIN/AEI/10.13039/501100011033 and by the "European Union NextGenerationEU/PRTR" is also acknowledged. L. V. was funded by the European Union's Horizon Europe Programme, through a FET Proactive research and innovation action under grant agreement No. 101084124 (DIAMOND). A. T. acknowledges the Project ECS00000024 "Ecosistemi dell'Innovazione"—Rome Technopole of the Italian Ministry of University and Research, public call no. 3277, PNRR—Mission 4, Component 2, Investment 1.5, financed by the European Union, Next GenerationEU. A. D. C. acknowledges the Project "Network 4 Energy Sustainable Transition—NEST", Spoke 1, Project code PE0000021, funded under the National Recovery and Resilience Plan (NRRP), Mission 4, Component 2, Investment 1.3—Call for tender No. 1561 of 11.10.2022 of Ministero dell'Università e della Ricerca (MUR); funded by the European Union—NextGenerationEU. This project has received funding from the European Union's Framework Programme for Research and Innovation Horizon Europe (2021–2027) under the Marie Sklodowska-Curie Grant Agreement No. 101068387 "EFESO".

Notes and references

1 J. Park, *et al.*, Controlled growth of perovskite layers with volatile alkylammonium chlorides, *Nature*, 2023, **616**, 724–730, DOI: **10.1038/s41586-023-05825-y**.

2 Q. Jiang, *et al.*, Surface reaction for efficient and stable inverted perovskite solar cells, *Nature*, 2022, **611**(7935), 278–283, DOI: **10.1038/s41586-022-05268-x**.

3 M. A. Green, E. D. Dunlop, J. Hohl-Ebinger, M. Yoshita, N. Kopidakis and X. Hao, Solar cell efficiency tables (Version 58), *Prog. Photovolt.: Res. Appl.*, 2021, **29**(7), 657–667, DOI: **10.1002/pip.3444**.

4 H. Choe, D. Jeon, S. J. Lee and J. Cho, Mixed or Segregated: Toward Efficient and Stable Mixed Halide Perovskite-Based Devices, *ACS Omega*, 2021, **6**(38), 24304–24315, DOI: **10.1021/acsomega.1c03714**.

5 T. T. Ava, A. Al Mamun, S. Marsillac and G. Namkoong, A review: thermal stability of methylammonium lead halide based perovskite solar cells, *Appl. Sci.*, 2019, **9**(1), 188, DOI: **10.3390/app9010188**.

6 S. Yang, *et al.*, Thiocyanate assisted performance enhancement of formamidinium based planar perovskite solar cells through a single one-step solution process, *J. Mater. Chem. A*, 2016, **4**(24), 9430–9436, DOI: **10.1039/c6ta02999j**.

7 J. Duan, *et al.*, Planar perovskite FAxMA1-xPbI3 solar cell by two-step deposition method in air ambient, *Opt. Mater.*, 2018, **85**, 55–60, DOI: **10.1016/j.optmat.2018.07.072**.

8 T. Zhang, *et al.*, Spontaneous low-temperature crystallization of α-FAPbI3 for highly efficient perovskite solar cells, *Sci. Bull.*, 2019, **64**(21), 1608–1616, DOI: **10.1016/j.scib.2019.08.029**.

9 J. Du, *et al.*, Crystallization Control of Methylammonium-Free Perovskite in Two-Step Deposited Printable Triple-Mesoscopic Solar Cells, *Sol. RRL*, 2020, **4**, 2000455, DOI: **10.1002/solr.202000455**.

10 J. W. Lee and N. G. Park, Two-step deposition method for high-efficiency perovskite solar cells, *MRS Bull.*, 2015, **40**(8), 654–659, DOI: **10.1557/mrs.2015.166**.

11 P. Fassl, *et al.*, Fractional deviations in precursor stoichiometry dictate the properties, performance and stability of perovskite photovoltaic devices, *Energy Environ. Sci.*, 2018, **11**(12), 3380–3391, DOI: **10.1039/c8ee01136b**.

12 Z. Yuan, *et al.*, Unveiling the synergistic effect of precursor stoichiometry and interfacial reactions for perovskite light-emitting diodes, *Nat. Commun.*, 2019, **10**(1), 1–9, DOI: **10.1038/s41467-019-10612-3**.

13 J. Yang, E. L. Lim, L. Tan and Z. Wei, Ink Engineering in Blade-Coating Large-Area Perovskite Solar Cells, *Adv. Energy Mater.*, 2022, **12**(28), 1–25, DOI: **10.1002/aenm.202200975**.

14 Y. Zhang, *et al.*, Mechanochemistry Advances High-Performance Perovskite Solar Cells, *Adv. Mater.*, 2022, **34**(6), 1–10, DOI: **10.1002/adma.202107420**.

15 G. S. Shin, Y. Zhang and N. G. Park, Stability of Precursor Solution for Perovskite Solar Cell: Mixture (FAI + PbI2)

versus Synthetic FAPbI3 Crystal, *ACS Appl. Mater. Interfaces*, 2020, **12**(13), 15167–15174, DOI: **10.1021/acsami.9b23086**.

16 J. Suo, *et al.*, Multifunctional sulfonium-based treatment for perovskite solar cells with less than 1% efficiency loss over 4,500-h operational stability tests, *Nat. Energy*, 2024, 1–12, DOI: **10.1038/s41560-023-01421-6**.

17 G. Tong, *et al.*, Removal of residual compositions by powder engineering for high efficiency formamidinium-based perovskite solar cells with operation lifetime over 2000 h, *Nano Energy*, 2021, **87**, 106152, DOI: **10.1016/j.nanoen.2021.106152**.

18 M. P. U. Haris, S. Kazim and S. Ahmad, Microstrain and Urbach Energy Relaxation in FAPbI3-Based Solar Cells through Powder Engineering and Perfluoroalkyl Phosphate Ionic Liquid Additives, *ACS Appl. Mater. Interfaces*, 2022, **14**(21), 24546–24556, DOI: **10.1021/acsami.2c01960**.

19 M. P. U. Haris, S. Kazim and S. Ahmad, Low-Temperature-Processed Perovskite Solar Cells Fabricated from Presynthesized CsFAPbI3Powder, *ACS Appl. Energy Mater.*, 2021, **4**(3), 2600–2606, DOI: **10.1021/acsaem.0c03160**.

20 B. Nambiraj, A. Kunka Ravindran, S. P. Muthu and R. Perumalsamy, Cost-Effective Synthesis Method: Toxic Solvent-Free Approach for Stable Mixed Cation Perovskite Powders in Photovoltaic Applications, *Small Methods*, 2024, 1–16, DOI: **10.1002/smtd.202400768**.

21 G. Kim, H. Min, K. S. Lee, D. Y. Lee, S. M. Yoon and S. Il Seok, Impact of strain relaxation on performance of a-formamidinium lead iodide perovskite solar cells, *Science*, 2020, **370**(6512), 108–112, DOI: **10.1126/science.abc4417**.

22 Y. Zhang, *et al.*, Achieving Reproducible and High-Efficiency (>21%) Perovskite Solar Cells with a Presynthesized FAPbI3 Powder, *ACS Energy Lett.*, 2020, 360–366, DOI: **10.1021/acsenergylett.9b02348**.

23 Y. Zhang, S. G. Kim, D. K. Lee and N. G. Park, CH3NH3PbI3 and HC(NH2)2PbI3 Powders Synthesized from Low-Grade PbI2: Single Precursor for High-Efficiency Perovskite Solar Cells, *ChemSusChem*, 2018, **11**(11), 1813–1823, DOI: **10.1002/cssc.201800610**.

24 Z. Li, M. Yang, J. S. Park, S. H. Wei, J. J. Berry and K. Zhu, Stabilizing Perovskite Structures by Tuning Tolerance Factor: Formation of Formamidinium and Cesium Lead Iodide Solid-State Alloys, *Chem. Mater.*, 2016, **28**(1), 284–292, DOI: **10.1021/acs.chemmater.5b04107**.

25 T. Bu, *et al.*, Lead halide-templated crystallization of methylamine-free perovskite for efficient photovoltaic modules, *Science*, 2021, **372**(6548), 1327–1332, DOI: **10.1126/science.abh1035**.

26 C. Harnmanasvate, R. Chanajaree, N. Rujisamphan, Y. Rong and R. Cheacharoen, Ambient Gas-Quenching Fabrication of MA-Free Perovskite Solar Cells Enabled by an Eco-Friendly Urea Additive, *ACS Appl. Energy Mater.*, 2023, **6**(20), 10665–10673, DOI: **10.1021/acsaem.3c01829**.

27 M. P. U. Haris, *et al.*, Probing proton diffusion as a guide to environmental stability in powder-engineered FAPbI3 and CsFAPbI3 perovskites, *Cell Rep. Phys. Sci.*, 2023, **4**(3), 101304, DOI: **10.1016/j.xcrp.2023.101304**.

28 R. Jiang, *et al.*, Low-Cost Fabrication of Efficient Perovskite Photovoltaics Using Low-Purity Lead Iodide via Powder Engineering, *ACS Appl. Mater. Interfaces*, 2023, **15**(17), 20958–20965, DOI: **10.1021/acsami.3c00358**.

29 T. Du, *et al.*, Precursor-Engineered Volatile Inks Enable Reliable Blade-Coating of Cesium–Formamidinium Perovskites Toward Fully Printed Solar Modules, *Adv. Sci.*, 2024, 2401783, DOI: **10.1002/advs.202401783**.

30 T. Niu, L. Chao, X. Dong, L. Fu and Y. Chen, Phase-Pure α-FAPbI3for Perovskite Solar Cells, *J. Phys. Chem. Lett.*, 2022, **13**(7), 1845–1854, DOI: **10.1021/acs.jpclett.1c04241**.

31 H. Chen, Y. Chen, T. Zhang, X. Liu, X. Wang and Y. Zhao, Advances to High-Performance Black-Phase FAPbI3 Perovskite for Efficient and Stable Photovoltaics, *Small Struct.*, 2021, **2**(5), 1–15, DOI: **10.1002/sstr.202000130**.

32 M. Du, *et al.*, High-Pressure Nitrogen-Extraction and Effective Passivation to Attain Highest Large-Area Perovskite Solar Module Efficiency, *Adv. Mater.*, 2020, **32**, 2004979, DOI: **10.1002/adma.202004979**.

33 Z. Li, *et al.*, Ammonia for post-healing of formamidinium-based Perovskite films, *Nat. Commun.*, 2022, **13**(1), 1–10, DOI: **10.1038/s41467-022-32047-z**.

34 Y. Deng, C. H. van Brackle, X. Dai, J. Zhao, B. Chen and J. Huang, Tailoring solvent coordination for high-speed, room-temperature blading of perovskite photovoltaic films, *Sci. Adv.*, 2019, **5**(12), 1–9, DOI: **10.1126/sciadv.aax7537**.

35 B. Wook Park, *et al.*, Publisher Correction: Stabilization of formamidinium lead triiodide α-phase with isopropylammonium chloride for perovskite solar cells, *Nat. Energy*, 2021, **6**, 419–428, DOI: **10.1038/s41560-021-00802-z**; B. Wook Park, *et al.*, *Nat. Energy*, 2021, **6**(8), 848, DOI: **10.1038/s41560-021-00844-3**.

36 H. Hu, M. Singh, X. Wan, J. Tang, C. W. Chu and G. Li, Nucleation and crystal growth control for scalable solution-processed organic-inorganic hybrid perovskite solar cells, *J. Mater. Chem. A*, 2020, **8**(4), 1578–1603, DOI: **10.1039/c9ta11245f**.

37 L. Vesce, *et al.*, Perovskite solar cell technology scaling-up: Eco-efficient and industrially compatible sub-module manufacturing by fully ambient air slot-die/blade meniscus coating, *Prog. Photovolt.: Res. Appl.*, 2024, **32**(2), 115–129, DOI: **10.1002/pip.3741**.

38 C. Ma, M. Grätzel and N. G. Park, Facet Engineering for Stable, Efficient Perovskite Solar Cells, *ACS Energy Lett.*, 2022, **7**(9), 3120–3128, DOI: **10.1021/acsenergylett.2c01623**.

39 X. Zhang, *et al.*, Precise Control of Crystallization and Phase-Transition with Green Anti-Solvent in Wide-Bandgap Perovskite Solar Cells with Open-Circuit Voltage Exceeding 1.25 V, *Small*, 2023, **19**(22), 1–9, DOI: **10.1002/smll.202208289**.

40 Y. Wang, *et al.*, Stitching triple cation perovskite by a mixed anti-solvent process for high performance perovskite solar cells, *Nano Energy*, 2017, **39**(July), 616–625, DOI: **10.1016/j.nanoen.2017.07.046**.

41 Z. Zhang, *et al.*, Anti-solvent engineering for efficient and stable perovskite solar cells with preferentially orientated 2-dimensional/3-dimensional heterojunctions, *Energy*

Environ. Sci., 2025, **18**(7), 3223–3234, DOI: 10.1039/D4EE05879H.

42 J. Li, *et al.*, Optimization of anti-solvent engineering toward high performance perovskite solar cells, *J. Mater. Res.*, 2019, **34**(14), 2416–2424, DOI: 10.1557/jmr.2019.122.

43 L. Vesce, *et al.*, Hysteresis-Free Planar Perovskite Solar Module with 19.1% Efficiency by Interfacial Defects Passivation, *Sol. RRL*, 2022, 2101095, DOI: 10.1002/solr.202101095.

44 E. G. Moloney, V. Yeddu and M. I. Saidaminov, Strain Engineering in Halide Perovskites, *ACS Mater. Lett.*, 2020, **2**(11), 1495–1508, DOI: 10.1021/acsmaterialslett.0c00308.

45 N. Wang, W. Liu and Q. Zhang, Perovskite-based nanocrystals: Synthesis and applications beyond solar cells, *Small Methods*, 2018, **2**(6), 1–19, DOI: 10.1002/smtd.201700380.

46 X. Hu, H. Wang, M. Wang and Z. Zang, Interfacial defects passivation using fullerene-polymer mixing layer for planar-structure perovskite solar cells with negligible hysteresis, *Sol. Energy*, 2020, **206**, 816–825, DOI: 10.1016/j.solener.2020.06.057.

47 C. Xin, *et al.*, Defects Healing in Two-Step Deposited Perovskite Solar Cells via Formamidinium Iodide Compensation, *ACS Appl. Energy Mater.*, 2020, **3**(4), 3318–3327, DOI: 10.1021/acsaem.9b02336.

48 J. W. Lee, *et al.*, The Interplay between Trap Density and Hysteresis in Planar Heterojunction Perovskite Solar Cells, *Nano Lett.*, 2017, **17**(7), 4270–4276, DOI: 10.1021/acs.nanolett.7b01211.

49 Y. Yang, *et al.*, Bi-functional additive engineering for high-performance perovskite solar cells with reduced trap density, *J. Mater. Chem. A*, 2019, **7**(11), 6450–6458, DOI: 10.1039/c8ta11925b.

50 M. V. Khenkin, *et al.*, Consensus statement for stability assessment and reporting for perovskite photovoltaics based on ISOS procedures, *Nat. Energy*, 2020, **5**(1), 35–49, DOI: 10.1038/s41560-019-0529-5.

51 C. Ding, *et al.*, Boosting Perovskite Solar Cells Efficiency and Stability: Interfacial Passivation of Crosslinked Fullerene Eliminates the 'Burn-in' Decay, *Adv. Mater.*, 2023, **35**, 2207656, DOI: 10.1002/adma.202207656.

52 P. Hang, *et al.*, Stabilizing Fullerene for Burn-in-Free and Stable Perovskite Solar Cells under Ultraviolet Preconditioning and Light Soaking, *Adv. Mater.*, 2021, **33**, 2006910, DOI: 10.1002/adma.202006910.

53 R. Singh, *et al.*, Danger in the Dark: Stability of Perovskite Solar Cells with Varied Stoichiometries and Morphologies Stressed at Various Conditions, *ACS Appl. Mater. Interfaces*, 2024, **16**(21), 27450–27462, DOI: 10.1021/acsami.4c04350.

54 R. Wang, M. Mujahid, Y. Duan, Z. K. Wang, J. Xue and Y. Yang, A Review of Perovskites Solar Cell Stability, *Adv. Funct. Mater.*, 2019, **29**(47), 1–25, DOI: 10.1002/adfm.201808843.

55 M. Kim, *et al.*, Methylammonium Chloride Induces Intermediate Phase Stabilization for Efficient Perovskite Solar Cells, *Joule*, 2019, **3**(9), 2179–2192, DOI: 10.1016/j.joule.2019.06.014.

56 F. Di Giacomo, L. A. Castriotta, F. U. Kosasih, D. Di Girolamo, C. Ducati and A. Di Carlo, Upscaling inverted perovskite solar cells: Optimization of laser scribing for highly efficient mini-modules, *Micromachines*, 2020, **11**(12), 1–13, DOI: 10.3390/mi11121127.

57 O. Almora, I. Zarazua, E. Mas-Marza, I. Mora-Sero, J. Bisquert and G. Garcia-Belmonte, Capacitive dark currents, hysteresis, and electrode polarization in lead halide perovskite solar cells, *J. Phys. Chem. Lett.*, 2015, **6**(9), 1645–1652, DOI: 10.1021/acs.jpclett.5b00480.

58 B. Chen, M. Yang, S. Priya and K. Zhu, Origin of J-V Hysteresis in Perovskite Solar Cells, *J. Phys. Chem. Lett.*, 2016, **7**(5), 905–917, DOI: 10.1021/acs.jpclett.6b00215.